RSC Advances

ROYAL SOCIETY OF CHEMISTRY

www.rsc.org/advances

Fabrication of carbon nanofibers with Si nanoparticle-stuffed cylindrical multi-channels via coaxial electrospinning and their anodic performance

Ho-Sung Yang[1+], Byoung-Sun Lee[1, 2+], Byeongchul You[1], Hun-Joon Sohn[1], and Woong-Ryeol Yu[1, *]

[1]*Department of Materials Science and Engineering (MSE) and Research Institute of Advanced Materials (RIAM), Seoul National University, 599 Gwanangno, Gwanak-gu, Seoul 151-742, Republic of Korea*

[2]*Samsung Advanced Institute of Technology (SAIT), 130 Samsungro, Suwon, Kyeonggido, 443-742, Republic of Korea*

Abstract

This paper reports on a fabrication method to manufacture cylindrically multi-channeled hollow carbon nanofibers (mcHCNFs). Polyacrylonitrile nanofibers with cylindrical multi-cores of poly(styrene-co-acrylontitrile) (SAN) were first electrospun using a specific nozzle and subsequently heat-treated, leaving vacant or silicone (Si)-encapsulated mcHCNFs. The latter was obtained by dispersing Si nanoparticles in the SAN solution. Investigations into the morphologies, microstructures, and material compositions of the resulting mcHCNFs demonstrated that Si-encapsulated multi-channels were formed in a controlled, uniform manner. The multi-channel effects were evaluated by characterizing the anodic properties of Si-encapsulated mcHCNFs using galvanostatic charge–discharge tests. More contacts between the Si nanoparticles and the carbon shell in the Si-encapsulated mcHCNFs brought about improved discharge capacity and capacity retention.

Keywords: Anodic performance, carbon nanofibers, cylindrical multi-channels, silicone-encapsulated

* Corresponding author. Tel.: +82 2 880 9096; fax: +82 2 883 8197
E-mail address: woongryu@anu.ac.kr (W.-R. Yu)
+These authors contributed equally to this work.

1. Introduction

Since the first observation of electrospinning behavior by Rayleigh in 1897 and a patent by Formhals in 1934 [1], the last several decades have brought the electrospinning process to the forefront in the manufacture of various functional products, such as filters [2], catalysts [2], sensors [3], scaffolds [4], and energy-storage devices [5], due to its simplicity with regard to the fabrication of one-dimensional (1-D) nanomaterials. Specifically, when an electrostatic force applied to a polymer drop is sufficient to overcome its surface tension, polymer jets are ejected that can be formed into nanofibers, ranging from 2 nm to several microns in size [1]. Various electrospinning techniques and designs have been researched for developing multi-functional nano-fibrous materials [2, 3].

'Coaxial' electrospinning, and its associated mechanism and characteristics, were first introduced by Loscertales et al. [6] and Sun et al. [7]. The process has since attracted considerable attention due to its application to the production of core-shell structure nanofibers [8, 9]. The core-shell structures exhibit excellent material properties (*e.g.*, spider silk and its associated mechanical strength [10]). Moreover, coaxial electrospinning facilitates nanofiber fabrication using materials known to have low spinnability (*e.g.*, oil [11], inorganic materials [12], conducting materials such as carbon nanotubes (CNTs) [13], and poly(3-hexylthiopene) (P3HT) [14]); in this case, the materials lacking spinnability are incorporated into the core and the highly spinnable materials are used for the shell. Recently, more sophisticated nanofiber structures have been demonstrated via coaxial electrospinning (*e.g.*, wire-in-tube [12, 15, 16] and multi-channel [17-19] structures).

Cylindrical multi-channeled nanofibers (*i.e.*, nanofibers with several cylindrical and continuous (vacant) cores) were researched to utilize the increased surface area due to the

multiple channels [20]. A polyvinylpyrrolidone (PVP)-Ti(O*i*Pr)$_4$ (TiO_2 precursor) solution and oil are commonly used as the shell and core materials for manufacturing multi-channeled nanofibers [18, 21]. Tang et al. demonstrated that the anode performance of electrospun TiO_2 nanofibers for lithium-ion batteries was improved by introducing a multi-channeled microstructure into the nanofibers via emulsion and single electrospinning [21]; however, precise control over the number of channels, their diameter, and distribution within the nanofibers was limited, due to sacrificial polymer islands. These polymer islands, which eventually formed into cores, are randomly sized and dispersed in the emulsion fluid during the electrospinning process. Zhao et al. reported multi-channeled TiO_2 nanofiber generation using a specially designed coaxial electrospinning process [18]. Multi-channeled hollow TiO_2 nanofibers, manufactured using coaxial electrospinning, exhibited improved performance as a photocatalyst for decomposition of acetaldehyde to CO_2 [18]. However, with the exception of these studies, there have been no additional systematic studies and few applications of the coaxial electrospinning process to multi-channeled nanofiber fabrication. Recently, there has been strong demand for cylindrical multi-channels in carbon nanofibers, due to their potential application to energy-storage devices.

Herein, we report on a fabrication method for manufacturing cylindrically multi-channeled carbon nanofibers; the cylindrical and continuous channels can be vacant or nanoparticle-stuffed. Polyacrylonitrile (PAN) nanofibers with cylindrical multi-cores of poly(styrene-co-acrylontitrile) (SAN) were manufactured by coaxial electrospinning, based on our previous research [22-24], using various material compositions, nozzle designs, and electrospinning conditions. Subsequent heat treatment was then applied to convert PAN into a carbonized shell and burn out the SAN, leaving multi-channeled hollow carbon nanofibers (mcHCNF) or silicone (Si) nanoparticles-encapsulated mcHCNF (SimcHCNF). Galvanostatic charge–

discharge experiments were performed to investigate the electrochemical performance of mcHCNFs and SimcHCNF, focusing on the effect of the multiple channels.

2. Experimental

2.1. Material preparations and processing methods

Polyacrylonitrile (PAN, M_w: 200,000 g mol^{-1}, Mitsui Chemical) and styrene-co-acrylonitrile (SAN, 28.5 mol% AN; M_w: 120,000 g mol^{-1}, Cheil Industries) were dissolved in *N,N*-dimethylformide (DMF, purity: 99.5%, Daejung Chemical) at 20 and 30 wt%, respectively. These PAN and SAN solutions were used as the carbonizing precursor for the shell and as a sacrificial core material, respectively, for mcHCNFs. Si nanoparticles (1 g, D < 100 nm, Aldrich) were added to the DMF solution and sonicated for 3 h. Note that the average diameter of Si nanoparticles was 110 nm (with the standard deviation of 49 nm). More specifically, the diameters of the nanoparticles mostly ranged from 50 to 150 nm (see Fig. S1). SAN (3 g) was then added to the Si/DMF solution and stirred at 80 °C for 5 h. This prepared solution was used as a core material to fabricate Si-encapsulated mcHCNF (SimcHCNF). The SAN and PAN solutions were used as the core and shell fluids; SAN is a thermally decomposable polymer, while PAN is a good carbonizing precursor [22].

The coaxial electrospinning conditions included an applied voltage of −18 kV, a tip-to-collector distance of 15 cm, and inner- and outer-solution flow rates of 0.5 and 1.25 mL h^{-1}, respectively. Multi SAN core/PAN shell nanofibers and multi Si-SAN core/PAN shell nanofibers were manufactured via coaxial electrospinning using a multi-coaxial nozzle, as shown in Fig. 1. The multi-SAN core was vertically injected while the PAN shell was supplied horizontally. Our previous reports demonstrated that the SAN core/PAN shell combination was highly suitable for multi-layered coaxial electrospinning, due to non-

precipitation, a large conductivity difference, use of the same solvent, immiscibility, and the various metamorphoses during heat treatment [22-24].

The multi-SAN core/PAN shell nanofibers were then thermally treated for stabilization and carbonization of the PAN shell. The stabilization was carried out at 270–300 °C for 1 h in air, followed by carbonization at 1000 °C for 1 h in a nitrogen atmosphere. The temperature rate was 10 °C min^{-1}. As reported earlier in a previous study, SAN can sustain the inner shape of the nanofibers up to 400 °C during heat treatment; however, above 400 °C, SAN is thermally decomposed [22]. Under these conditions, the carbonization of the PAN shell continues, resulting in a turbostratic carbon structure. Multi Si-SAN core/PAN shell nanofibers were converted into SimcHCNFs by the thermal treatment.

2.2. Morphological and electrochemical characterization

The surface and inner morphologies of the resulting nanofibers were investigated using a field-emission scanning electron microscope (FE-SEM) (JSM-7600F, JEOL Korea) and a high-resolution transmission electron microscope (HR-TEM, JEM–3000F). Thermogravimetric analysis (TGA) (Mettler Toledo) and wide-angle X-ray diffraction (WAXD) (wavelength: 0.154 nm, New D8 Advance, Bruker) studies were carried out to quantify the Si nanoparticles encapsulated in the HCNF and to investigate the microstructure of the Si in the nanofibers, respectively.

To characterize the anodic properties of the manufactured nanofibers, galvanostatic charge–discharge tests were carried out over a voltage range of 0.01–1.5 V for a charge–discharge current of 50 mA g^{-1}. For coin-cell preparation, the active material (nanofibers), carbon black (conducting agent), and polyamide imide (PAI, binder), in a 7:2:1 weight ratio, were

dissolved in N-methyl pyrrolidinone (NMP). The slurry was then pasted onto a copper foil and dried at 200 °C for 4 h. Lithium foil was used as the counter and reference electrodes, and 1-M $LiPF_6$ in ethylene carbonate (EC)/diethylene carbonate (DEC) (5:5 (v/v), PANAX) was used as the electrolyte [25].

3. Results and discussion

Two-channeled hollow carbon nanofibers (2cHCNF) were manufactured using the process described in Fig. 1. To fabricate a four-channeled hollow carbon nanofiber (4cHCNF), the same electrospinning system as that used for the 2cHCNF was used for the 4cHCNF, with the exception of the nozzle system; a core nozzle with four orifices was used in this case. Two key factors were considered in the design of an efficient nozzle system. First, the distance between the PAN-solution inlet and the multi-SAN core outlet was controlled, such that the horizontal flow of the PAN solution did not affect the vertical flow of the multi-SAN core solution. Second, the core nozzle supplying the multi-SAN cores was retracted inside the PAN-shell nozzle. This so-called core-cut nozzle system was used to stabilize the hydrodynamic effects of the two solutions before forming a Taylor cone, leading to better electrospinnability and multi-layered nanofiber formation [12, 13, 22-24].

3.1 Morphologies of multi-channeled hollow carbon nanofibers

Morphologies of cylindrically multi-channeled hollow carbon nanofibers (mcHCNFs) were characterized as shown in Fig. 2 and Fig. 4 (a) and (b). SEM (Fig. 2) and TEM (Fig. 4) images of 2cHCNFs (Fig. 2 (a,c) and 4 (a,c), respectively) and 4cHCNFs (Fig. 2(b,d) and 4(b,d), respectively) clearly showed the uniform formation of circular two- and four-channels in the carbon nanofibers, as well as uniform, continuous, multi-channeled CNFs manufactured over a long range (Fig. 2 (c) and (d)). The shape of the holes or their

eccentricity represent the proximity of an ellipse to a circle (*i.e.*, the closer the eccentricity value is to zero, the more circular the ellipse). The eccentricities of the 2cHCNF and 4cHCNF were 0.45 and 0.29, respectively, implying that more circular channels formed for the 4cHCNF (Fig. 2(b)). This was probably due to the symmetric arrangement of the core needles; *i.e.*, four needles were symmetrically introduced for the 4cHCNF, leading to symmetric inner (four) components in the as-spun precursor nanofibers and circular holes in the carbonized nanofibers. The elliptical shape of the 2cHCNF was caused by the low symmetric flow behavior of the PAN solution during electrospinning (as indicated by the arrows in Fig. 2(a)). The diameters of the 2cHCNF and 4cHCNF were 671.0 nm (± 102.2 nm) and 642.0 nm (± 107 nm), respectively (Table 1). Note that the hole size of the two nanofibers was quite different, due to the asymmetric flow of the PAN shell (*e.g.*, the hole size of the 4cHCNF was smaller than that of the 2cHCNF (Table 1)).

3.2 Fabrication of Si-encapsulated multi-channeled hollow carbon nanofibers

To increase the functionality of multi-channeled HCNFs, Si nanoparticles were encapsulated in the cylindrical channels inside the mcHCNFs. Fig. 3(a) and (b) show typical mcHCNFs containing Si nanoparticles encapsulated within two and four cylindrical channels, respectively. As the number of cylindrical channels increased, the uniformity of the nanofibers gradually deteriorated due to the aggregation of Si nanoparticles and their large size. The Si-encapsulated four-channeled HCNFs (Si4cHCNF) in Fig. 3 (d) appeared to have more Si beads, compared with the Si-encapsulated two-channeled HCNFs (Si2cHCNF) in Fig. 3(a, c), due in part to the small channel diameter of Si4cHCNF (222.1 nm (± 74.7 nm)). Note that the channel diameter of Si2cHCNF was 480.7 nm (± 195.6 nm). Since fewer Si nanoparticles filled the Si4cHCNF, it was smaller in diameter (690.8 nm (± 145.2 nm)) than that of Si2cHCNF (1097.6 nm (± 338.7 nm)). TEM images of the nanofibers (Fig. 4(c) and

(d)) showed non-uniform filling of the Si nanoparticles in the channels; this was attributed to the size of the Si nanoparticles used in this study. The average size of Si nanoparticles was at around 100 nm, which was large relative to the channel diameter. Si nanoparticles smaller in size than the ones used in this study are expected to fill the channels more uniformly; this hypothesis will be investigated in a future study. For comparison purposes, Si-encapsulated one-channeled HCNFs (Si1cHCNFs), the so-called core-shell HCNFs, were manufactured using the same coaxial electrospinning conditions, with the exception of the nozzle system, in which a two concentric-cylinder nozzle system was used. Fig. 5 shows Si nanoparticles of various sizes encapsulated in the HCNF.

SimcHCNFs were manufactured using coaxial electrospinning and subsequent heat treatment. Side reactions between Si and C may occur during the heat-treatment step; this was investigated using WAXD. Fig. 6 shows that the Si core remained in the crystalline phase after the heat treatment, while the PAN shell successively transformed into the carbonized structure. In the WAXD curves, typical peaks associated with turbostratic carbon and crystalline silicon crystals are (002) and (10) [26] and (111), (220), (311), (422), and (511) [24], respectively. The lack of a silicon carbide peak confirmed that the crystalline phase of Si was maintained throughout the heat treatment, without any side reactions [13].

SimcHCNFs were characterized using Raman spectroscopy. The Raman spectra in Fig. S2 shows a turbostratic carbon structure at 1380 cm^{-1} (D-peak) and 1583 cm^{-1} (G-peak) [27] and a silicon crystalline structure at 520 cm^{-1} [12]. Note that the D peak is related to defects in carbon and the G peak corresponds to the sp^2 hybrid structure. The lower the value of the I_D/I_G ratio (*i.e.*, the ratio of the intensity of the D and G peaks), the higher the degree of carbonization.

The I_D/I_G ratio of SimcHCNFs did not change significantly with changes in the cross-section (0.76, 0.74, and 0.76, respectively, in Table S1).

TGA was carried out to determine the amount of Si nanoparticles encapsulated in the nanofibers (Fig. S3). The weight fractions of Si and C are shown in Table 2. As the number of cylindrical channels increased, the Si content in the nanofibers decreased. This was an unexpected outcome, because the Si and C precursors were supplied equally during the coaxial electrospinning process (thus, the resulting nanofibers should possess the same amount of each element). The coaxial electrospinning mechanism can explain the mismatch. With coaxial electrospinning, the shell fluid forms an electrified jet from its Taylor cone when the applied electrostatic force overcomes the surface tension of the shell fluid, whereas the core fluid is viscously dragged by the moving shell fluid [28]. The dragging force by the shell fluid became weaker as the number of the channels increased, because the surface area of the multi-channels was large compared with that of a single channel. This resulted in a small drag force per unit area and a small throughput of the core material. Another possible explanation for the discrepancy in the nanofiber content may be associated with the sizes of the Si nanoparticles and the diameter of the channels. Because the size of the Si nanoparticles was relatively large as mentioned earlier, the likelihood of the Si nanoparticles being encapsulated decreased with the channel diameter.

3.3 Anodic properties of Si-encapsulated multi-channeled hollow carbon nanofibers

The electrochemical performances of mcHCNFs were evaluated using a galvanostatic charge–discharge test. As the number of channels increased, the first discharge capacity increased slightly. For 1cHCNF, 2cHCNF, and 4cHCNF, the resulting capacities were 352, 388, and 370 mAh g^{-1}, respectively (Fig. 7(a)). Such an increase was attributable to the

increased surface area of the mcHCNFs. The discharge capacities of the nanofibers after 40 cycles converged to 220 mAh g^{-1} with good Coulombic efficiency (~98%).

The effect of Si nanoparticles encapsulated in mcHCNFs on their electrochemical performance was investigated (Fig. 7(b)). The discharge capacities of Si1cHCNF, Si2cHCNF, and Si4cHCNF were 1044, 876, and 777 mAh g^{-1}, respectively. This result is somewhat puzzling in that the additional number of channels should increase the conductive path of the Si nanoparticles and improve the buffering effect of the carbon shell. However, our results did not reveal this structural effect. Direct assessment of the structural effect was not possible given the current data. The Si content was highest in Si1cHCNF (Table 2); thus, it provided the highest capacities. This issue will be discussed further using normalized data.

The differential capacity curves of SimcHCNFs are shown in Fig. 7(c) and (d). In Fig. 7(c), a broad peak developed near 0.8 V in the first lithiation curve (below zero), which was related to the formation of the solid electrolyte interface and Li-ion insertion into the mesopores in the carbon shell. The peak below 0.2 V was associated with the amorphization of crystalline Si and the reversible intercalation of the Li ions into the carbon shell. The deintercalation peaks of the Li ions from the carbon and silicon were also observed near 0.09 and 0.44 V, respectively. As the cycles proceeded, the Li ions were reversibly inserted and extracted. Fig. 7(d) shows the broad peaks associated with the lithiation and delithiation behavior of the amorphous silicon: the lithiation peaks developed at 0.24 and 0.09 V, while the delithiation peaks evolved at 0.27 and 0.44 V [24, 29]. It is noteworthy that the reversible lithiation/delithiation of the carbon shell appeared at 0.01 and 0.09 V, respectively [24].

The structural effect of SimcHCNFs was investigated by calculating their discharge capacities based on the incorporated Si content. The specific capacity of the Si–carbon composite anode, with respect to the Si content, was calculated by subtracting the contribution of carbon from the total capacity and then dividing the remainder by the Si weight fraction [12, 29-31]. Fig. 8 shows the highest capacity (2615 mAh g^{-1}) for the Si4cHCNF; the other two nanofibers exhibited a lower capacity (2506 and 2276 mAh g^{-1} for Si1cHCNF and Si2cHCNT, respectively). The capacity of Si4cHCNF was highest, even though its actual Si content was the lowest among the three nanofibers tested (Table 2); this was attributed to the structural effect of having more contact points between the Si and carbon due to the enlarged surface. Additionally, Si4cHCNF exhibited the maximum retention capacity (72.6%) after the 50th cycle, whereas slightly lower values (66.82% and 67.61%, respectively) were observed for Si1cHCNF and Si2cHCNF. The normalized discharge capacity and retention demonstrated indicated the structural influence of the SimcHCNFs. Such a structural effect was not observed in Si2cHCNF, which showed a lower specific capacity than Si1cHCNF. This can be explained in terms of the dimensions of the Si2cHCNF. The diameter of Si2cHCNF (1097.6 nm (± 338.7 nm)) was larger than that of Si1cHCNF (710.1 nm (± 139.2 nm)) and Si4cHCNF (690.8 nm (± 145.2 nm)) [32]. Additionally, the shell of Si2cHCNF (214.6 nm (± 46.2 nm)) was thicker than that of Si1cHCNF and Si4cHCNF, indicating that the Li ions have a longer diffusion path from the shell to the Si nanoparticles in Si2cHCNF, compared with Si1cHCNF and Si4cHCNF [33]. This, in turn, contributed to the lower capacity of the Si2cHCNFs without the contribution of positive structural effects from the two channels in the HCNFs. Note that this dimensional constraint was due mainly to the large Si nanoparticles, as explained in Section 3.1, as opposed to the smaller Si nanoparticles that were able to create this structural effect in SimcHCNFs.

The structural stability after cycles is one of the most important factors for determining the performance of Si/carbon composite electrodes because the volume change of Si during the electrochemical reactions causes the deterioration of the structure and performance of the composite electrodes. We proved the structural stability of Si core/carbon shell nanofiber electrodes by conducting the contact-lithiation test [24], measuring the mechanical properties of the pristine and electrochemically reacted carbon nanofibers [27], and comparing the morphologies of the pristine and cycled Si/carbon composite nanofibers [12]. Here, the morphologies of Si2cHCNFs and Si4cHCNFs after 10 cycles were investigated using FE-SEM (see Fig. S4). As we expected, the multi-channel structures of Si2cHCNFs and Si4cHCNFs were well-maintained regardless of the silicon nanoparticles' volume changes during the electrochemical reactions.

4. Conclusion

mcHCNFs were manufactured successfully using a coaxial electrospinning process and subsequent heat treatment. The structural effect of mcHCNFs, resulting from their cylindrical multi-channels, was investigated by incorporating Si nanoparticles into the channels. The electrochemical performance of SimcHCNFs was then characterized, demonstrating that cylindrical multi-channels in CNFs were structurally efficient in terms of enlarging the conductive path of Si nanoparticles and enhancing the buffering effect of the carbon shell, as evidenced by the improved discharge capacity and its retention in galvanostatic charge–discharge testing.

Acknowledgement

This research was supported by the Mid-career Researcher Program through a NRF grant funded by the Korea government (MSIP) (2013R1A2A2A01067717).

Notes

Electronic Supplementary Information (ESI) available: the size distribution of silicon nanoparticles, Raman spectra, thermogravimetric analyses, morphologies of SimcHCNFs after cycles, and I_D/I_G ratio of SimcHCNFs are provided in Supplementary Information. See DOI: 10.1039/b000000x/

References

1. N. Bhardwaj and S. C. Kundu, *Biotechnol. Adv.*, 2010, **28**, 325-347.
2. Z.-M. Huang, Y. Z. Zhang, M. Kotaki and S. Ramakrishna, *Compos. Sci. Technol.*, 2003, **63**, 2223-2253.
3. W. E. Teo and S. Ramakrishna, *Nanotechnology*, 2006, **17**, R89.
4. X. M. Mo, C. Y. Xu, M. Kotaki and S. Ramakrishna, *Biomaterials*, 2004, **25**, 1883-1890.
5. Z. Dong, S. J. Kennedy and Y. Wu, *J. Power Sources*, 2011, **196**, 4886-4904.
6. I. G. Loscertales, A. Barrero, I. Guerrero, R. Cortijo, M. Marquez and A. M. Gañán-Calvo, *Science*, 2002, **295**, 1695-1698.
7. Z. Sun, E. Zussman, A. L. Yarin, J. H. Wendorff and A. Greiner, *Adv. Mater.*, 2003, **15**, 1929-1932.
8. K. S. Mayya, D. I. Gittins, A. M. Dibaj and F. Caruso, *Nano Lett.*, 2001, **1**, 727-730.
9. S. O. Obare, N. R. Jana and C. J. Murphy, *Nano Lett.*, 2001, **1**, 601-603.
10. F. Vollrath and D. P. Knight, *Nature*, 2001, **410**, 541-548.
11. J. T. McCann, D. Li and Y. Xia, *J. Mater. Chem.*, 2005, **15**, 735-738.
12. B.-S. Lee, H.-S. Yang, H. Jung, S.-Y. Jeon, C. Jung, S.-W. Kim, J. Bae, C.-L. Choong, J. Im, U. I. Chung, J.-J. Park and W.-R. Yu, *Nanoscale*, 2014, **6**, 5989-5998.
13. B.-S. Lee, S.-B. Son, J.-H. Seo, K.-M. Park, G. Lee, S.-H. Lee, K. H. Oh, J.-P. Ahn and W.-R. Yu, *Nanoscale*, 2013, **5**, 4790-4796.
14. S. Lee, G. D. Moon and U. Jeong, *J. Mater. Chem.*, 2009, **19**, 743-748.
15. E. Hosono, Y. Wang, N. Kida, M. Enomoto, N. Kojima, M. Okubo, H. Matsuda, Y. Saito, T. Kudo, I. Honma and H. Zhou, *ACS Appl. Mater. Interfaces*, 2009, **2**, 212-218.
16. H. Chen, N. Wang, J. Di, Y. Zhao, Y. Song and L. Jiang, *Langmuir*, 2010, **26**, 11291-11296.
17. Y. Zhao, X. Cao and L. Jiang, *J. Am. Chem. Soc.*, 2007, **129**, 764-765.
18. T. Zhao, Z. Liu, K. Nakata, S. Nishimoto, T. Murakami, Y. Zhao, L. Jiang and A. Fujishima, *J. Mater. Chem.*, 2010, **20**, 5095-5099.
19. W. Li, C.-Y. Cao, C.-Q. Chen, Y. Zhao, W.-G. Song and L. Jiang, *Chem. Commun.*, 2011, **47**, 3619-3621.
20. H. Chen, J. Di, N. Wang, H. Dong, J. Wu, Y. Zhao, J. Yu and L. Jiang, *Small*, 2011, **7**, 1779-1783.
21. K. Tang, Y. Yu, X. Mu, P. A. van Aken and J. Maier, *Electrochem. Commun.*, 2013, **28**, 54-57.
22. B.-S. Lee, K.-M. Park, W.-R. Yu and J. Youk, *Macromol. Res.*, 2012, **20**, 605-613.
23. B.-S. Lee, S.-B. Son, K.-M. Park, W.-R. Yu, K.-H. Oh and S.-H. Lee, *J. Power Sources*, 2012, **199**, 53-60.
24. B.-S. Lee, S.-B. Son, K.-M. Park, J.-H. Seo, S.-H. Lee, I.-S. Choi, K.-H. Oh and W.-R. Yu, *J. Power Sources*, 2012, **206**, 267-273.
25. W.-S. Kim, Y. Hwa, J.-H. Jeun, H.-J. Sohn and S.-H. Hong, *J. Power Sources*, 2013, **225**, 108-112.
26. B.-S. Lee, S.-B. Son, K.-M. Park, G. Lee, K. H. Oh, S.-H. Lee and W.-R. Yu, *ACS Appl. Mater. Interfaces*, 2012, **4**, 6702-6710.

27. B.-S. Lee, J.-H. Seo, S.-B. Son, S. C. Kim, I.-S. Choi, J.-P. Ahn, K. H. Oh, S.-H. Lee and W.-R. Yu, *ACS Nano*, 2013, **7**, 5801-5807.
28. A. K. Moghe and B. S. Gupta, *Polym. Rev.*, 2008, **48**, 353-377.
29. S.-H. Ng, J. Wang, D. Wexler, K. Konstantinov, Z.-P. Guo and H.-K. Liu, *Angew. Chem. Int. Ed.*, 2006, **45**, 6896-6899.
30. S.-L. Chou, Y. Zhao, J.-Z. Wang, Z.-X. Chen, H.-K. Liu and S.-X. Dou, *J. Phys. Chem. C*, 2010, **114**, 15862-15867.
31. A. Magasinski, P. Dixon, B. Hertzberg, A. Kvit, J. Ayala and G. Yushin, *Nat. Mater.*, 2010, **9**, 353-358.
32. C. Kim, K. S. Yang, M. Kojima, K. Yoshida, Y. J. Kim, Y. A. Kim and M. Endo, *Adv. Funct. Mater.*, 2006, **16**, 2393-2397.
33. C. Jiang, E. Hosono and H. Zhou, *Nano Today*, 2006, **1**, 28-33.

Table 1. Overall diameter, shell thickness, and hole diameter of multi-channeled hollow carbon nanofibers (HCNFs) and multi-channeled Si-encapsulated HCNFs (SimcHCNFs).

Sample	Diameter (nm)	Shell thickness (nm)	Hole diameter (nm)
2cHCNF	671.0 ± 102.2	49.6 ± 21.2 (147.8 ± 37.6)	310.3 ± 65.7
4cHCNF	642.0 ± 107.0	58.8 ± 20.1	204.8 ± 40.5
Si1cHCNF	710.1 ± 139.2	126.8 ± 32.1	497.3 ± 98.9
Si2cHCNF	1097.6 ± 338.7	61.3 ± 24.5 (217.6 ± 46.2)	480.7 ±195.6
Si4cHCNF	690.8 ± 145.2	61.8 ± 21.4	222.1 ± 74.7

Table 2. Weight fractions of silicon and carbon calculated using thermogravimetric analysis.

Sample	Si1cHCNF	Si2cHCNF	Si4cHCNF
Si	32.2%	25.9%	18.1%
Carbon	67.8%	74.1%	81.9%

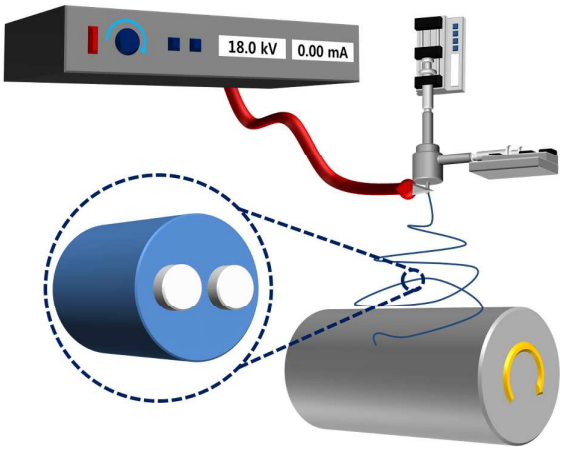

(a)

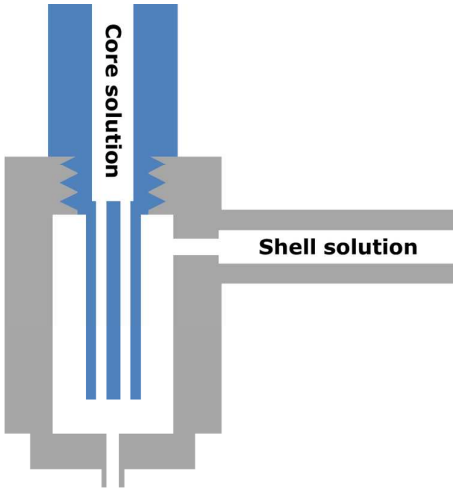

(b)

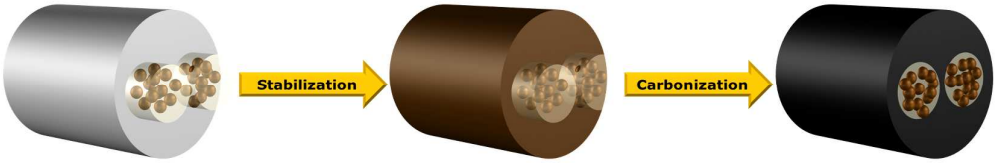

(c)

Figure 1. Schematic illustrations of (a) the coaxial electrospinning system for manufacturing cylindrically multi-channeled carbon nanofibers (mcCNFs), (b) the cross-section of the coaxial nozzle, and (c) the structural changes of the coaxially electrospun nanofibers in accordance with the thermal treatment applied.

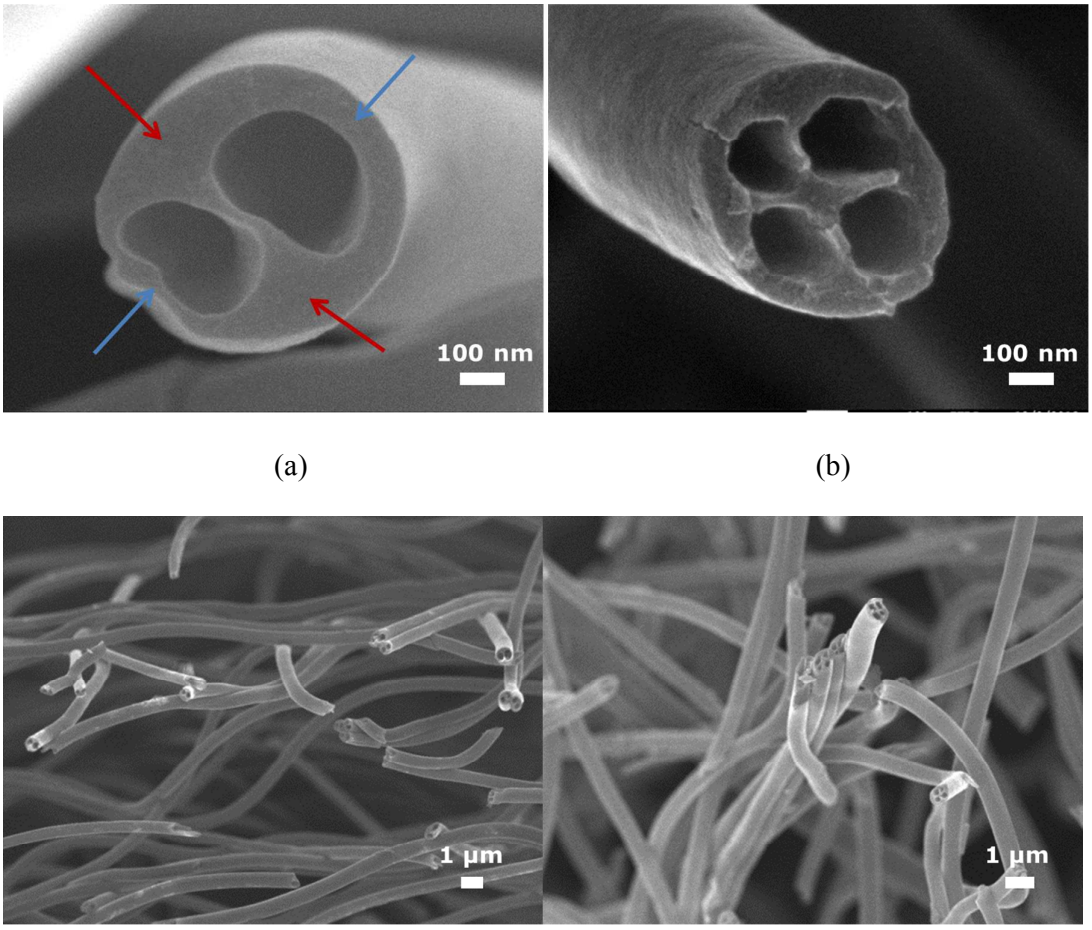

(a) (b)

(c) (d)

Figure 2. Morphological characterizations of multi-channeled, hollow CNFs (mcHCNFs). Field emission-scanning electron microscopy (FE-SEM) images of (a,c) two-channel HCNF (2cHCNF) and (b,d) a four-channel HCNF (4cHCNF) at high and low resolution.

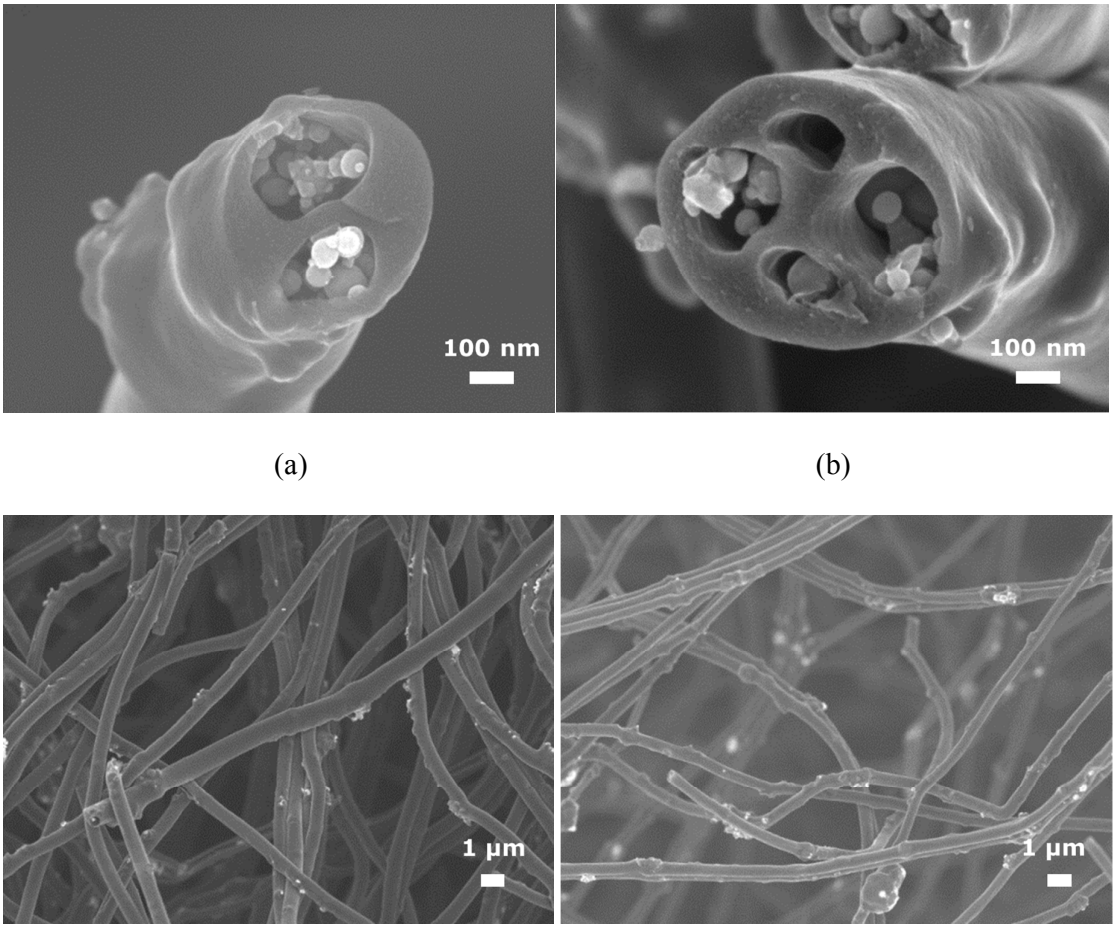

Figure 3. Morphological characterizations of multi-channeled and Si-encapsulated HCNFs. FE-SEM images of (a,c) Si2cHCNF and (b,d) Si4cHCNF at high and low resolution.

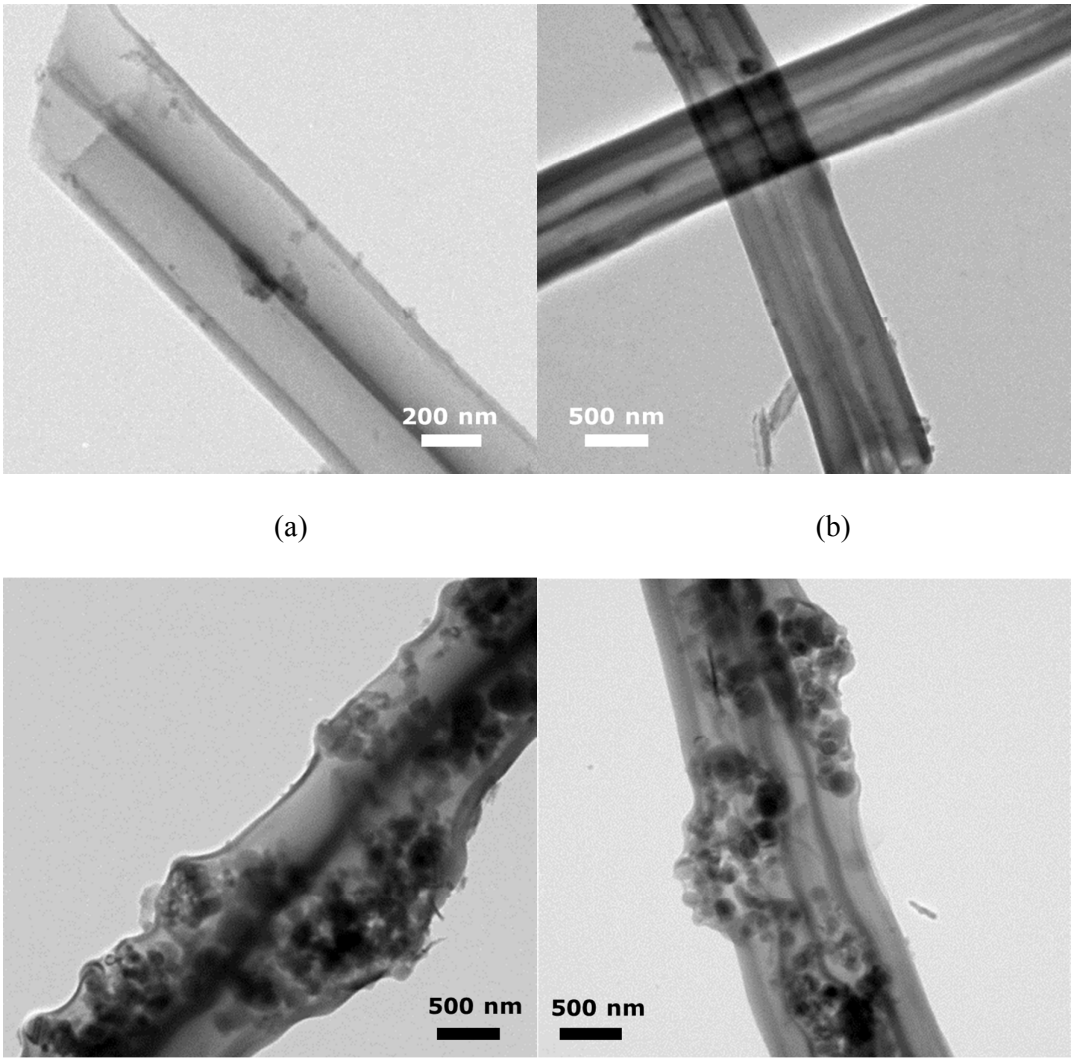

Figure 4. Transmission electron microscopy (TEM) images of (a) 2cHCNF, (b) 4cHCNF, (c) Si2cHCNF, and (d) Si4cHCNF.

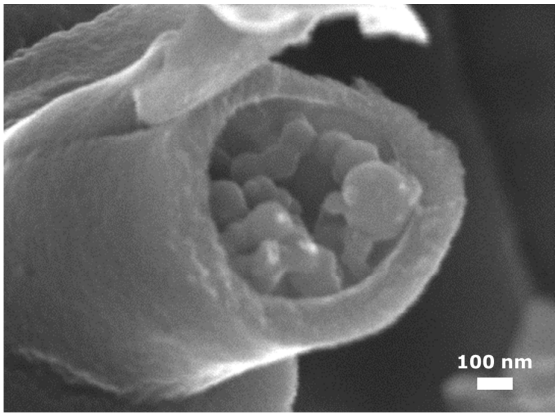

Figure 5. FE-SEM image of Si-encapsulated HCNF (Si1cHCNF). For comparison purposes, it was manufactured using coaxial electrospinning and thermal treatment.

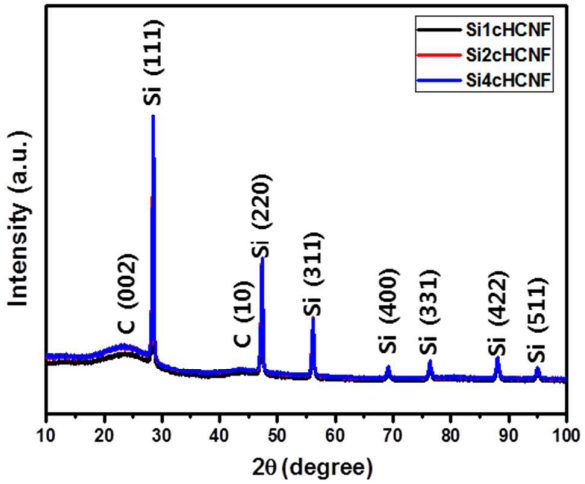

Figure 6. Wide-angle X-ray diffraction (WAXD) pattern of SimcHCNFs.

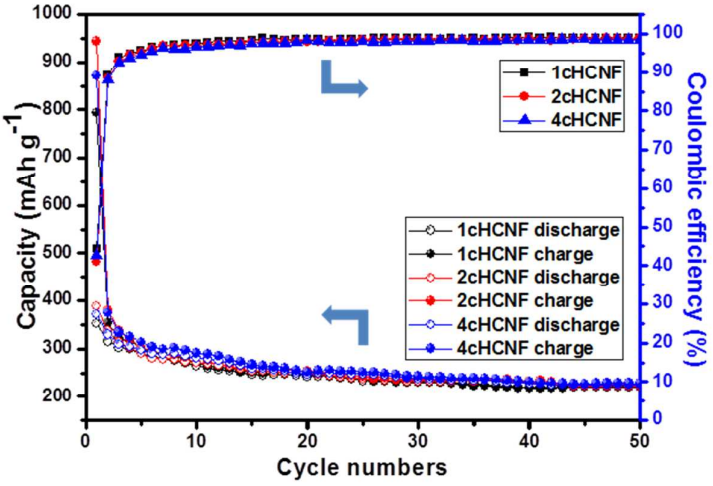

(a)

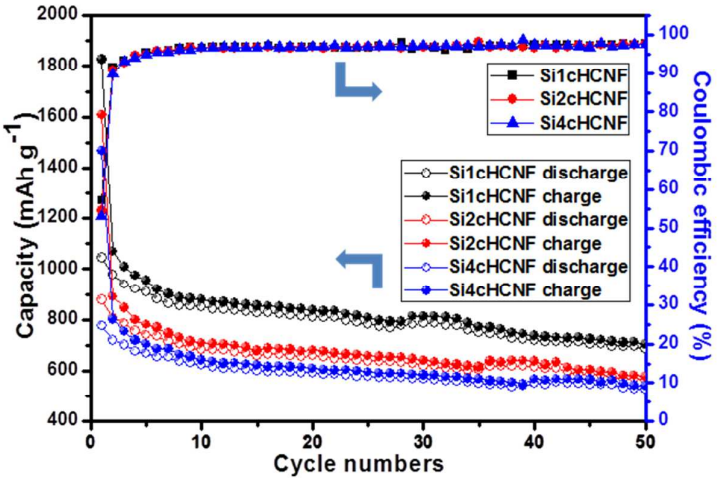

(b)

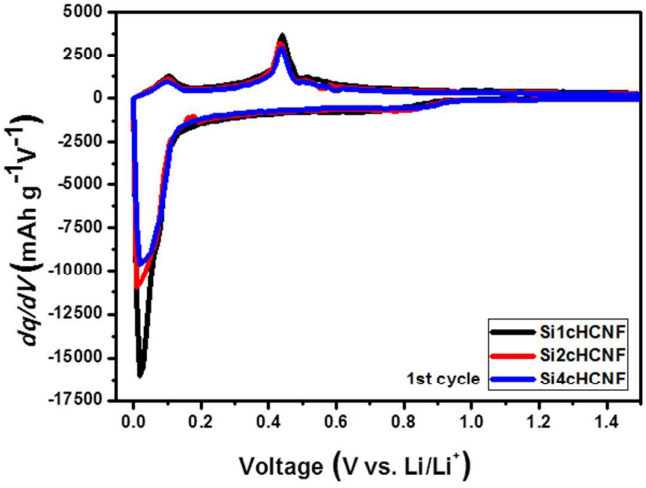

(c)

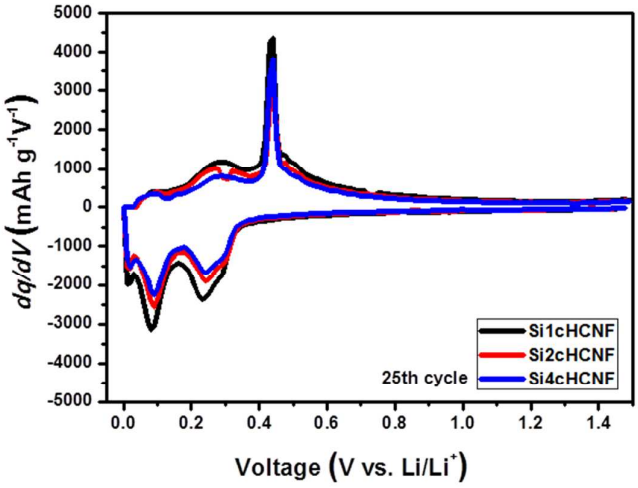

(d)

Figure 7. Comparison of the cycling performances of (a) multi-channeled HCNFs (1cHCNF, 2cHCNFs, and 4cHCNFs) and (b) multi-channeled Si-encapsulated HCNFs (Si1cHCNFs, Si2cHCNFs, and Si4cHCNFs). (c) and (d) Differential capacity curves of SimcHCNFs for the 1st and 25th cycles.

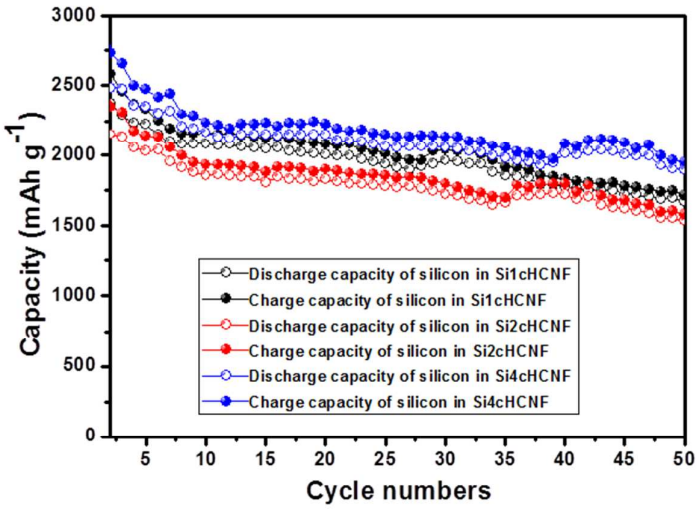

Figure 8. Cycling performances of SimcHCNFs, normalized with respect to the Si content.

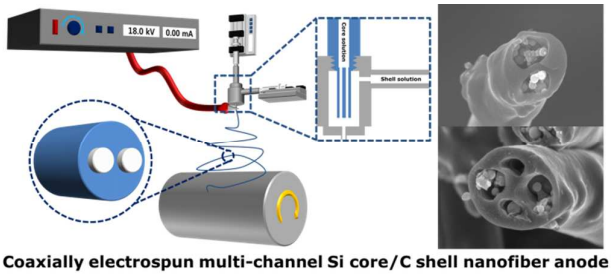

Coaxially electrospun multi-channel Si core/C shell nanofiber anode

Si-encapsulated, multi-channeled carbon nanofiber anode, manufactured using coaxial electrospinning, shows improved electrochemical performance.